Shear Effects on the Phase Diagrams of Solutions of Highly Incompatible Polymers in a Common Solvent. 2. Experiment and Theory

Cora Krause, Roland Horst, and B. A. Wolf*

Institut für Physikalische Chemie, Johannes Gutenberg-Universität, Jakob-Welder-Weg 13, D-55099 Mainz, Germany

Received July 1, 1996; Revised Manuscript Received October 11, 1996[⊗]

ABSTRACT: Cloud point temperatures (T_{cp}) were measured at different constant shear rates for three representatives of the ternary system cyclohexanone/polystyrene/poly(*n*-butyl methacrylate) (CHO/PS/PBMA) by means of a newly constructed rheo-optical apparatus that can be operated in the temperature range from 0 to 100 °C up to maximum shear rates of 1440 s^{-1} and maximum stresses of 384 Pa. In all cases one observes an extension of the homogeneous region as the shear rate $\dot{\gamma}$ is raised. With the system CHO/PS 196w/PBMA 2050 (the figures denote the molar masses of the polymers in kilograms/mole) the effects become maximum for high concentrations of PBMA, where the demixing temperatures increase by more than 25 °C per 100 s^{-1}. For a pronounced predominance of one polymer in the mixture, T_{cp} is a linear function of $\dot{\gamma}$ in the entire range of shear rates. At blend compositions in between, the slope of T_{cp} *versus* $\dot{\gamma}$ is largest at the lowest shear rates and diminishes as $\dot{\gamma}$ is increased until the dependence becomes linear again at sufficiently large values. Possible effects of polymolecularity were studied by exchanging the broadly distributed PS 196w against the narrowly distributed PS 207; no differences beyond experimental error could be detected. A substitution of the high molecular weight PBMA 2050 by the lower molecular PBMA 335 leads to a pronounced reduction of the effects; in this case the extent of shear-induced mixing passes a minimum for a blend composition of approximately 1:1. Phase diagrams of the flowing systems of interest were also calculated theoretically on the basis of a generalized Gibbs energy of mixing (value for stagnant solutions plus energy stored under stationary conditions in the sheared state) by direct minimization of this quantity. The information concerning equilibrium and rheological behavior required for that purpose was obtained as described in part 1 of this series. The sign and magnitude of all theoretically predicted effects plus their variation with molar masses and composition are in very good agreement with the experimentally observed features of shear-induced changes of the phase state. Possible reasons for the lack of complete quantitative agreement are discussed.

Introduction

Observations concerning shear influences on the phase separation behavior of polymer-containing systems have a long history. Many investigations on flow influences on thermodynamic properties can be found in the secondary literature;[1] there are reports on a pronounced increase of the homogeneous region upon flow (shear-induced mixing)[2−5] as well as on the opposite, namely, phase separation upon shearing (shear-induced demixing).[6−10] With some systems the sign of the effects changes with composition or shear rate,[11] and for others there are indications for the formation of closed miscibility gaps.[12,13]

Probably the above list of observations is not yet complete and the theoretical understanding[14,15] of the great variety of phenomena still constitutes a challenge. Work in the field of the phase behavior of flowing systems is also attractive in view of its great practical importance. For example, a shear-induced homogenization in the course of a suspension polymerization, or conversely, a shear-induced demixing in the course of a polymerization—supposed to proceed in a homogeneous medium—may change the properties of the product dramatically. Similarly, a phase state of a polymer blend in an extruder differing from that at rest will likely cause difficulties.[13]

The first section of this paper deals with the measurement of shear effects on the phase separation of a ternary system made up of two highly incompatible polymers and a solvent which is thermodynamically good for both components. The second section is devoted to corresponding theoretical calculations; they are based on an approach which generalizes the Gibbs energy of mixing by adding the energy the flowing system can store in the stationary state.[16] This procedure has in the past already turned out to be surprisingly predictive and could account—at least qualitatively—for all effects that were detected experimentally so far. With the present ternary system it could only be applied thanks to a calculation method[17] that does not require chemical potentials. In the third and final section of this paper, the experimental finding are compared with theoretical predictions.

Table 1. List of Substances Used and Sample Characteristics

	PBMA 2050	PBMA 335	PS 196w	PS 207
M_w/kg mol^{-1}	2050	335	196	207
M_n/kg mol^{-1}	1780	325	66	204
$U = M_w/M_n - 1$	0.15	0.03	1.95	0.02[a]

[a] Data of supplier.

Experimental Section

The samples of polystyrenes (PS) and of poly(*n*-butyl methacrylate)s (PBMA) utilized in this work are shown in Table 1; information concerning the provenance of the system can be obtained from part 1 of this series.[18] Cyclohexanone (CHO), purchased from Aldrich (Steinheim, Germany) with 99.8% purity, is a thermodynamically good solvent for both kinds of polymers.

The following relations served for the computation of the numbers of segments (N_i) of the different components from

* E-mail: wolf@pc-ak-wolf.chemie.uni-mainz.de.

[⊗] Abstract published in *Advance ACS Abstracts,* January 15, 1997.

S0024-9297(96)00944-8 CCC: $14.00

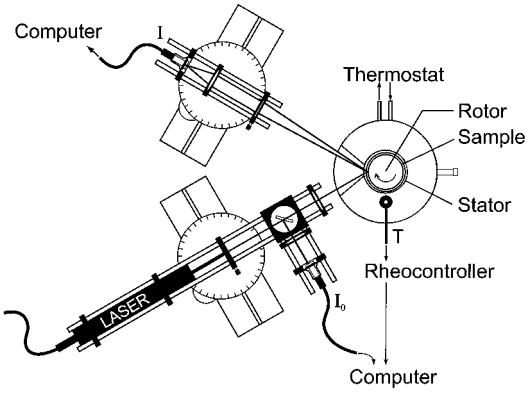

Figure 1. Scheme of the rheo-optical apparatus used for the simultaneous measurement of the turbidity and the viscosity of liquids; I_o and I are the intensities of the primary laser beam before and after passing through the solution twice.

their densities; the data for the polymers stem from ref 19. Densities and viscosities of CHO were taken from ref 20.

$$\rho_{PBMA}/(g\ cm^{-3}) = 1.0720 - 6.80 \times 10^{-4}(T/°C) \quad (1)$$

$$\rho_{PS}/(g\ cm^{-3}) = 1.0865 - 6.190 \times 10^{-4}(T/°C) + 1.360 \times 10^{-7}(T/°C)^2 \quad (2)$$

$$\rho_{CHO}/(kg\ m^{-3}) = 964.51 - 0.891(T/°C) \quad (3)$$

$$\ln(\eta_{CHO}/Pa\ s) = -11.93 + 1720.69(K/T) \quad (4)$$

Rheo-Optical Apparatus. The apparatus presented schematically in Figure 1 was assembled from commercially available optical parts using components of the shear-rate-controlled Haake rheometer (Rheocontroller RC 20, Rotovisco RV 20, measuring device M5). Its central part consists of a rotor−stator system (Searle type) which allows the simultaneous measurement of the viscosity of the liquid contained in the gap and of the ratio I/I_o, the intensity I of the light having passed the solution twice divided by I_o, the intensity of the primary laser beam. For this purpose, it was necessary to replace a part of the stator by a glass tube of 0.5 cm height, where the laser beam can pass through the sample.

In its present configuration, the apparatus can be operated in the T interval from 10 to 100 °C. With the smaller rotor (MV2, diameter 36.80 mm), the maximum shear stress that can be reached amounts to 384 Pa; with the larger rotor (MV1, 40.08 mm), this value is 324 Pa. Sample temperatures were increased linearly (0.1 K/min) and the measured turbidities and viscosities automatically recorded and processed in a computer. A typical example for the primary data obtained with the rheo-optical device is shown in Figure 2. Due to our experimental practice (varying the composition of system by adding more solvent to concentrated solutions of PS and PBMA in CHO), the results are presented in terms of w^*_{PBMA}, the weight fraction of PBMA in the blend PS/PBMA ($w^*_{PBMA} = w_{PBMA}/(w_{PS} + w_{PBMA})$), and of w_{pol}, the overall weight fraction of the polymer ($w_{pol} = w_{PS} + w_{PBMA}$).

The above graph demonstrates how cloud points were determined from the development of turbidity as the solutions are heated (lowest critical solution temperatures): The intercept of the linear parts of I/I_o as a function of T, observed within the homogeneous region and as one enters the two-phase regime, was taken as the cloud point temperature (T_{cp}). With many systems studied in the literature,[11] the segregation of a second phase can be monitored quite accurately (particularly at low shear rates) by a discontinuity in the temperature dependence of the viscosity (η). In the present case, however, this method turned out to be inapplicable for most shear rates, as becomes obvious from the temperature dependence of the viscosity also depicted in Figure 2. This feature is due to the fact that the viscosities of the two coexisting phases are too similar to "hide" the more viscous material in the disperse

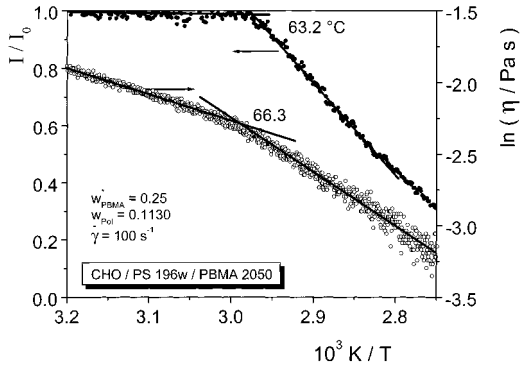

Figure 2. Temperature dependence of I/I_o, the ratio of light intensities, and of viscosity, η, measured with the apparatus schematically depicted in Figure 1. The system, composition, and shear rate, $\dot{\gamma}$, are indicated in the graph; w_{pol} is the sum of the weight fractions of the polymers and w^*_{PBMA} is the weight fraction of PBMA in the binary polymer blend.

phase; the almost matching η values result from tie lines which run almost parallel to the PS/PBMA edge of the Gibbs phase triangle (cf. Figure 6 of part 1).

Results and Discussion

As with the experiments concerning the equilibrium and the rheological behavior of the different representatives of the system CHO/PS/PBMA reported in part 1,[18] the emphasis of the present study on shear influences is on CHO/PS 196w/PBMA 2050. Some orienting experiments are also performed with a system where the rather polydisperse PS 196w is exchanged against the narrowly distributed PS 207 and with a system where the lower molecular weight PBMA 335 replaces PBMA 2050. To minimize the number of graphs, the results of the theoretical calculations are presented together with the experimental findings.

Measured Shear Influences. How the cloud point temperatures of the system CHO/PS 196w/PBMA 2050 depend on shear rate $\dot{\gamma}$ is shown in Figure 3a−e. This sequence of graphs demonstrates that the effects ($\Delta T_{cp}/\Delta\dot{\gamma}$) pass a pronounce maximum as w^*_{PBMA} is raised from 0.09 to 0.91. For a given blend composition and 20 °C, the maximum polymer concentration in the homogeneous solutions is for stagnant systems determined by the corresponding cloud point curve.

For very low and very high w^*_{PBMA} values, a shear rate of 400 s^{-1} increases the cloud point temperatures of the stagnant solutions by ca. 20−30 °C (extension of homogeneous region/shear-induced mixing) in an approximately linear manner (cf. Figure 3a,e). In the intermediate range of w^*_{PBMA}, the effects are much more pronounced. Here the dependencies T_{cp} versus $\dot{\gamma}$ are linear only at higher shear rates, and the effects are particularly striking at low $\dot{\gamma}$ values (Figure 3b−d). With solutions of the blend containing 75 wt % of PBMA, the change in the demixing temperature is for some polymer concentrations so large that one leaves the temperature range that is accessible with the present apparatus before the end of the available shear rate scale is reached (Figure 3d). For this blend composition the effects are for some polymer concentrations so large that shaking a turbid solution in an ordinary test tube causes it to become totally transparent. A more detailed discussion of the influences of the composition of the ternary system on the magnitude of shear effects will be given as experiment and theory are compared.

To study possible influences of the comparatively large polymolecularity of PS 196w, measurements were

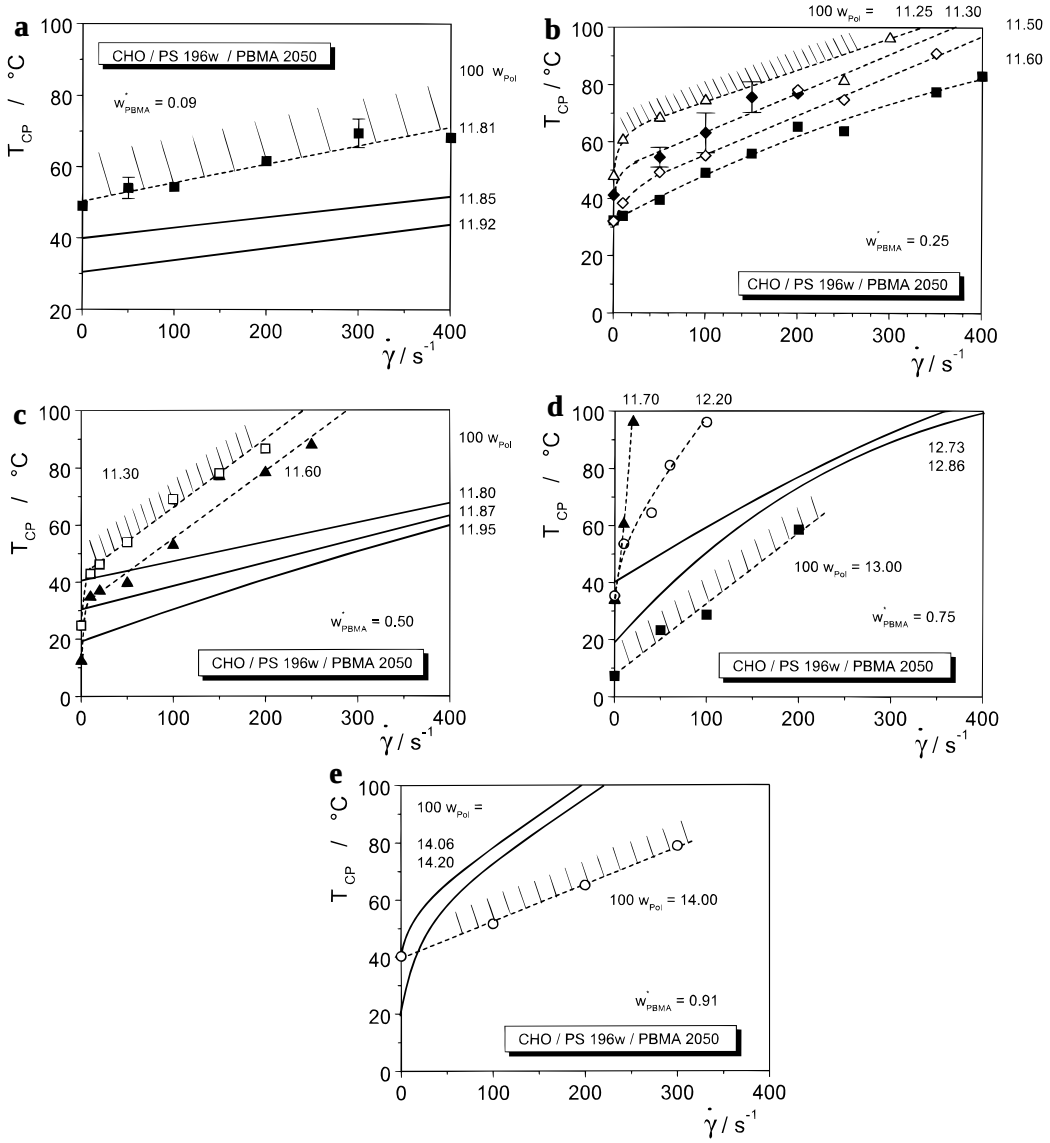

Figure 3. Shear rate dependencies of the cloud point temperatures for solutions of PS 196w and PBMA 2050 in CHO and constant composition. The weight fractions of the polymers are indicated in the graphs. Symbols and broken lines stand for measurements; the solid lines are calculated as described in the text.

performed with the narrowly distributed PS 207 and $w^*_{PMBA} = 0.09$, i.e. for a large predominance of PS in the blend so that the effects should become most obvious. The results lack any indication for particular consequences of a broader molecular weight distribution; the shear influences are practically identical. The fact that effects, which should according to thermodynamic expectation exist, do not show up is probably due to the large incompatibility of the polymers which suppresses differences in chain length.

The role of the molecular mass of PBMA on the extent of shear-induced mixing was examined for PBMA 335 instead of PBMA 2050. Some representative results are given in Figure 4; they demonstrate that the effects are for solutions rich in PBMA still quite obvious, despite an approximately 6-fold reduction of chain length. However, this time the consequences of shear are much more prominent as one component (in particular the PS) predominates in the blend, whereas they almost vanish in the middle part of the composition range, in contrast to the situation encountered with PBMA 2050, where the situation was just the opposite.

The results shown in the above graphs for the lower molecular weight PBMA and that given in Figure 3a−e

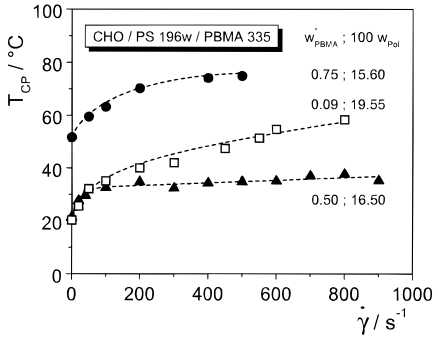

Figure 4. Same plot as Figure 3 but for PBMA 335 instead of PBMA 2050.

for the higher molecular weight PBMA contain implicit information on extrema in the sensitivity of the demixing temperature to shear as a function of blend composition. This situation can be seen explicitly in Figure 5, where the slope ($\Delta T_{cp}/\Delta\dot{\gamma}$) of the linear parts of the aforementioned graphs is plotted as a function of w^*_{PBMA}.

An example for the shift in the isothermal cloud point curve caused by shear, as obtained from the measure-

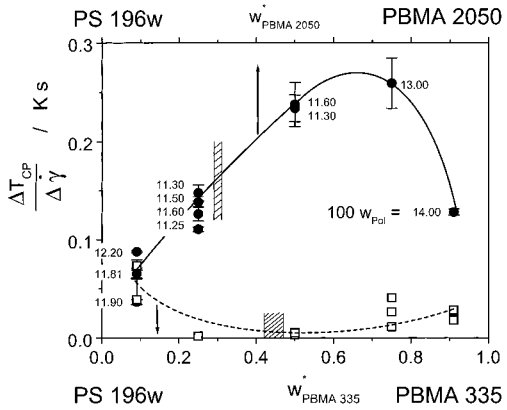

Figure 5. Sensitivity of the cloud point temperature to shear, as measured by $\Delta T_{cp}/\Delta\dot\gamma$ as a function of the composition of the binary polymer blend. ΔT_{cp} is the increase in the cloud point temperature associated with a certain increase $\Delta\dot\gamma$ of the shear rate as read from the linear parts of the dependencies shown in Figures 3 and 4. The total polymer concentrations in the ternary system are written at the data points; the approximate locations of the critical conditions are indicated by hatching.

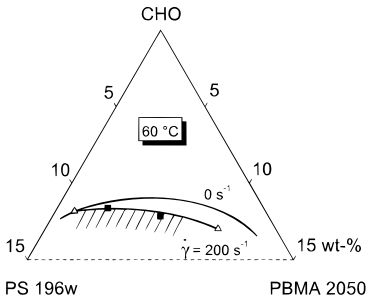

Figure 6. Experimental phase diagram of the system CHO/PS 196w/PBMA 2050 for 60 °C. The upper line represents the cloud point curve of the stagnant solutions (cf. Figure 2, part 1), the lower one gives the results for a shear rate of 200 s^{-1} as obtained from Figure 3a−e. Open symbols stand for interpolated data and filled symbols for extrapolated data.

ments presented in Figure 3a−e, is given in Figure 6. for 60 °C. This phase diagram discloses that shear-induced mixing is much more pronounced for mixtures that contain more of the higher molecular weight PBMA and less of the lower molecular weight PS.

Calculated Shear Influences. The computation of phase diagrams for flowing systems is based on the generalized Gibbs energy, $G\dot\gamma$, which was introduced[16] as the sum of G_z, the Gibbs energy of the stagnant equilibrium system, and E_s, the energy the sheared system stores in its stationary state. For the segment molar generalized Gibbs energy of mixing this relation reads

$$\overline{\Delta G_{\dot\gamma}} = \overline{\Delta G_z} + \overline{\Delta E_s} \tag{5}$$

where $\overline{\Delta E_s}$ is defined as

$$\overline{\Delta E_s} = \overline{E_s} - (\varphi_1\overline{E_{s,1}} + \varphi_2\overline{E_{s,2}}) \tag{6}$$

Equation 5 turned out to be very capable for the description of the actual behavior of polymer-containing systems.[11] This qualification can be rationalized from the fact that the second term is normally at least three orders of magnitude less than the first term so that one encounters a near equilibrium situation.

Table 2. Parameters Describing the Concentration Dependence of $g_{PS,PBMA}$ (Eq 10)

a	$b \times 10^3$	$c \times 10^3$	T/°C
0.37328	5.300	8	20
0.37378	5.330	8	30
0.37428	5.240	8	40
0.37539	5.200	8	60
0.37650	5.110	8	80
0.37755	5.333	8	100

For the present calculations $\overline{\Delta G_z}$ is described by the well known Flory−Huggins expression in which φ_i stands for the volume fractions of the components

$$\frac{\overline{\Delta G_z}}{RT} = \sum_{i=1}^{3}\frac{1}{N_i}\varphi_i \ln \varphi_i + \sum_{i=1}^{2}\sum_{j=i+1}^{3} g_{ij}\varphi_i\varphi_j \tag{7}$$

The numbers of segments (N_i) of the polymers are calculated from their molar volumes by dividing them by the molar volume of the solvent, V_{CHO}, which is taken to consist of one segment. The binary interaction parameters for solvent/polymer (g_{ij}) were determined experimentally as reported in part 1.[18] They read, in terms of $\varphi^*_i = \varphi_i/(\varphi_i + \varphi_j)$, the composition referring to the binary subsystems i/j:

$$g_{CHO,PS} = -0.2750 + \frac{0.89}{(1 - 0.20\varphi^*_{PS})} \tag{8}$$

$$g_{CHO,PBMA} = 0.2536 + \frac{0.44}{(1 - 0.54\varphi^*_{PBMA})} \tag{9}$$

They are in good approximation independent of temperature. For the polymer/polymer interaction parameter the following relation was obtained[18]

$$g_{PS,PBMA} = \frac{a + b\varphi^*_{PS}(1 - \varphi^*_{PS})}{(1 - c\varphi^*_{PS})} \tag{10}$$

The values of a, b, and c for the different temperatures of present interest are collected in Table 2.

The segment molar stored energy $\overline{E_s}$ can be calculated from the measured zero shear viscosities η_0 according to[21]

$$\overline{E_s} = V_{CHO}\frac{\tau_0}{\eta_0}(\eta\dot\gamma)^2 \tag{11}$$

where τ_0 is the characteristic viscometric relaxation time. The composition and temperature dependence of η_0 (in Pa s, T in K) can for the present system be described by[18]

$$\ln \eta_0 = A + Bw^*_{PBMA} \tag{12}$$

$$A = \left(-10.8 + \frac{1481}{T}\right) + 33.8w_{pol} - 56.1{w_{pol}}^2$$

$$B = 0.93 + \left(95.0 - \frac{183 \times 10^2}{T}\right)w_{pol} - \left(636 - \frac{1636 \times 10^2}{T}\right){w_{pol}}^2$$

τ_0 can be determined if $\eta(\dot\gamma)$ is known in a sufficient range of shear rates where the non-Newtonian behavior is observed. Since we didn't reach these high shear rates, in particular for solutions rich in PS, τ_0 was

approximated by the Rouse relaxation time[22] τ_R

$$\tau_R = \frac{6}{\pi^2}(\eta_0 - \eta_{CHO})\frac{M_{pol}}{c_{pol}RT} \quad (13)$$

In this equation c_{Pol} is the entire polymer concentration and M_{pol} the mean molar mass of the blend

$$c_{pol} = \frac{w_{pol}}{\sum_i \frac{w_i}{\rho_i}} \quad (14)$$

$$M_{pol} = (w^*_{PS}M_{PS} + w^*_{PBMA}M_{PBMA}) \quad (15)$$

The viscosity of the pure solvent, η_{CHO}, is given by eq 4.

Phase diagrams for sheared systems can be calculated on the basis of eqs 4−15 by direct minimization of the generalized Gibbs energy. This method, which is particularly advantageous for multicomponent systems and/or complicated concentration dependencies of interaction parameters, has already been described in detail[17] for stagnant systems. It avoids the calculation of chemical potentials and yields spinodal lines and critical points by means of test tie lines monitoring the effects of minute concentration fluctuations. The composition of coexisting phases is determined by calculating the maximum reduction of the Gibbs energy for mixtures of fixed overall composition. The phase diagrams resulting with the present systems for different shear rates $\dot{\gamma}$ are shown in parts a and b of Figure 7 for 20 and 60 °C, respectively.

The most striking feature of the theoretical results is the pronounced enlargement of the homogeneous region on the PBMA side of the Gibbs phase triangle as the shear rates become larger. The explanation for the much less obvious effects on the PS side lies in the largely different chain lengths of the two polymers. Another interesting peculiarity is the counterclockwise rotation of the (generalized) tie lines and a corresponding shift in the (generalized) critical points. This behavior is comprehensible since the solvent quality of CHO improves with $\dot{\gamma}$ in the case of PBMA but not so for PS.

Since the shear rate dependence of the viscosity is neglected, i.e. η is set equal to η_0, only shear-induced mixing can be calculated. At 60 °C one observes a similar shift of the binodal curves, however, at much higher shear rates than at 20 °C, since the viscosities are lower at the higher temperature.

Comparison between Experiment and Theory. Prior to quantitative considerations, whether some fundamental experimental features of shear influences can be understood qualitatively in terms of the generalized Gibbs energy of mixing is investigated.

According to the generalized Gibbs energy of mixing formulated in eq 5, the sign of shear effects is governed by the curvature of E_s as a function of composition, and the size of the changes should increase with the magnitude and curvature of the stored energy. From the fact that all solutions under investigation exhibit shear-induced mixing, one can conclude that the curvature is always positive. From the fact that the viscosity of the solutions increases as polymer concentrations and/or polymer masses are raised, it is obvious that E_s increases equivalently.

According to the present considerations the actual shift in the cloud point temperatures reflects the curvature of $\overline{\Delta G_z}$ as compared with the curvature and magnitude of $\overline{\Delta E_s}$. Assuming—in accord with the experience for ternary systems solvent/polymer A/polymer B—that the critical range (where the curvature of $G(\varphi)$ is almost zero) expands widely around the critical composition, the maximum and the minimum shown in Figure 5 can be interpreted in terms of the viscosity of the solutions near the conditions of phase separation. For the system CHO/PS 196w/PBMA 2050 the increase of η_0 upon a movement along the cloud point curve toward the PBMA corner of the phase triangle (cf. Figures 2 and 8 of part 1[18]) is so pronounced that the maximum effects are markedly shifted out of the critical region where the system is most sensitive to shear. On the other hand, with the system CHO/PS 196w/PBMA 335 the viscosity and thus the stored energy are still small in the critical range of the system due to the lower molar mass of PBMA and can only cause tiny effects. Larger shear influences show up, however, as one moves along the cloud point curve to either polymer edge in the phase triangle (cf. Figure 2 and 8 of part 1[18]), increasing the polymer concentration and consequently E_s.

The quantitative comparison of shear effects is performed in terms of shifts in the cloud point concentrations at constant temperature and in terms of changes of T_{cp} for solution of constant composition. As can be judged from the isothermal phase diagrams depicted in Figure 7b for different shear rates and from the experimental observation given in Figure 6, the agreement is quite reasonable.

Some examples for a quantitative comparison between experiment and theory for constant composition of the solutions are presented in Figure 3a−e in terms of the shear rate dependence of the cloud point temperatures. Calculated and measured lines are given for as similar as possible overall polymer concentration due to the present measurement and calculation procedures, exact matches are difficult.

In view of numerous simplifications of the theoretical treatment, experiment and theory agree quite well. Even the observation that T_{cp} increases linearly with $\dot{\gamma}$ in the entire experimentally accessible range of shear rates for some blend compositions, whereas this dependence is preceded by a steep increase for others (cf. Figure 3b,c), is reproduced by the theoretical calculation; the values of w^*_{PBMA} at which the particular behavior shows up differ, however, from the experimental data.

A vertical shift, i.e. displacement along the temperature axis, of the theoretical curves is caused by differences between the measured and calculated cloud point curve of the stagnant system (cf. Figure 7 of part 1). The slopes of the theoretical and experimental curves fit very well for $w^*_{PBMA} = 0.09$ and 0.75 (Figure 3a,d). For a value of 0.91 (Figure 3e), the slope of the theoretical curve is much larger. This is based on the neglect of shear thinning, which would reduce the stored energy and thus the shear influences on the phase separation behavior. The reason for the discrepancy at $w^*_{PBMA} = 0.50$ (Figure 3c) may be the polydispersity of PS. At this blend composition, the maximum of the cloud point curve is reached and the difference between the experimental cloud point curve and experimental binodal line becomes particularly obvious (Figure 6 of part 1).

In particular, the simplifications are as follow:

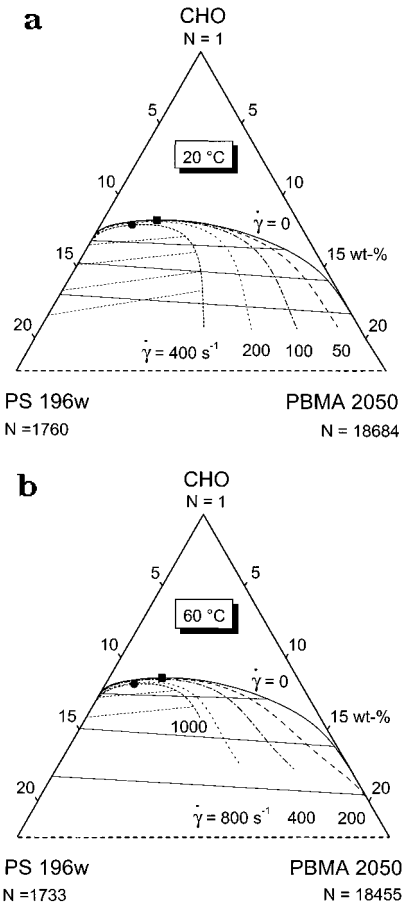

Figure 7. Theoretical phase diagrams of the system CHO/PS 196w/PBMA 2050 for (a) 20 and (b) 60 °C. The full lines show the cloud point curves for the equilibrium case, the broken ones those calculated for the indicated shear rates. The full square indicates the equilibrium critical point; the full circle gives the generalized critical point at 400 s^{-1}.

(1) The modeling of G_z neglects the fact that the polymers are not monodisperse. Especially for PS 196w, the polydispersity is so high that exact calculations have to account for this fact.

(2) The interaction parameters for the binary subsystem solvent/polymer are assumed to be independent of temperature. Furthermore, a possible dependence of $g_{CHO,PBMA}$ on the molar mass of PBMA is disregarded.

(3) The simplifications concerning the stored energy are much more serious. E_s is postulated to be half the trace of the stress tensor,[23] equal to the first normal stress difference N_1. Since we have not measured N_1, it is calculated from the shear dependence of the viscosity with further assumptions.[24] One of these is that the relaxation time is calculated as the Rouse relaxation time.

(4) For the mixtures with high PBMA contents, it was assumed that the Newtonian behavior observed for the other solutions is maintained. Although the extent of shear thinning is not very pronounced, this postulate is unrealistic. i.e. N_1 and E_s no longer scale with $\dot{\gamma}^2$ and N_1 becomes less than in the Newtonian case.[25] These considerations could explain the deviations between experiment and theory on the PBMA side of the phase diagram.

Conclusions

The present investigation has demonstrated the usefulness of the theoretical concept developed for the description of shear effects also for the modeling of a ternary system using the concentration dependent interaction parameters required for a realistic description of reality in the absence of shear. The theoretical predictions are in good qualitative agreement with the experimental findings; there is, however, still some quantitative discrepancy. Disregarding experimental inaccuracies, the explanation could lie in neglects on the theoretical side, in an improper modeling of the stored energy, or in principal deficiencies of the present approach. Clarification of this item and expansion of the work to elongational flow and to variable hydrostatic pressures is planned for the future.

Acknowledgment. We are very grateful to the DFG (Deutsche Forschungsgemeinschaft) for financial support.

References and Notes

(1) Søndergaard, K.; Lyngaae-Jørgensen, J. *Rheo-Physics of Multiphase Polymer Systems: Characterization by Rheo-Optical Techniques*; Technomic Publishing Company, Inc.: Lancaster, PA, 1995.
(2) Silberberg, A.; Kuhn, W. *Nature* **1952**, *170*, 450; *J. Polym. Sci.* **1954**, *13*, 21.
(3) Kammer, H. W., Kummerloewe, C.; Kressler, J.; Melior, J. P. *Polymer* **1991** *32*, 1488.
(4) Han, C. C. *Macromol. Symp.* **1996**, *101*, 157.
(5) Rector, L. P.; Mazich, K. A.; Carr, S. H. *J. Macromol. Sci.-Phys.* **1988**, *B27*, 421.
(6) Ver Strate, G.; Philippoff, W. *Polym. Lett. Ed.* **1974**, *12*, 267.
(7) Mani, S.; Malone, M. F.; Winter, H. H. *Macromolecules* **1992**, *25*, 5671.
(8) Hindawi, I. A.; Higgins, J. S.; Weiss, R. A. *Polymer* **1992**, *33*, 2522.
(9) Fernandez, M. L.; Higgins, J. S.; Richardson, S. M. *Trans. Inst. Chem. Eng.* **1993**, *71*, 239.
(10) Larson, R. G. *Rheol. Acta* **1992**, *31*, 497.
(11) Krämer-Lucas, H.; Schenck, H.; Wolf, B. A. *Makromol. Chem.* **1988**, *189*, 1613 and 1627.
(12) Fernandez, M. L.; Higgins, J. S.; Horst, R.; Wolf, B. A. *Polymer* **1995** *36*, 149.
(13) Aelmans, N. J. J.; Reid, V. M. C. In *Extended Abstracts of the European Symposium on Polymer Blends*, Maastricht, May 12−15 1996; p 153.
(14) Onuki, A.; Hashimoto, T. *Macromolecules* **1989**, *22*, 879.
(15) Criado-Sancho, M.; Casas-Vazquez, J.; Jou, D. *Polymer* **1995**, *36*, 4107.
(16) Wolf, B. A. *Macromolecules* **1984**, *17*, 615.
(17) Horst, R. *Macromol. Theory Simul.* **1995**, *4*, 449.
(18) Krause, C.; Wolf, B. A. *Macromolecules* **1997**, *30*, 885.
(19) Petri, H.-M. Ph.D. thesis, Johannes Gutenberg-Universität, Mainz, Germany, 1994.
(20) BASF Industriechemikalien, Technisches Merkblatt, Anon rein, M 2162 d, Oktober 1992.
(21) Horst, R.; Wolf B. A. *Rheol. Acta* **1994**, *33*, 99.
(22) Rouse, P. E.; *J. Chem. Phys.* **1953**, *21*, 1272.
(23) Marucci, G. *Trans. Soc. Rheol.* **1972**, *16*, 321.
(24) Bird, R. B.; Abdel-Khalik, S. J.; Hassager, O. *Polym. Eng. Sci.* **1974**, *14*, 859.
(25) Pahl, M.; Gleissle, W.; Laun, H.-M. *Praktische Rheologie der Kunststoffe und Elastomere*; VDI-Verlag: Düsseldorf, 1995.

MA9609442